Iminosugar infusions in rats. Additional Wistar and ZDF rats were implanted with ig and iv catheters. After a 7-10 day recovery period food was removed overnight on the evening before the day of the experiment, at the same time rats were also connected to a metal collar, allowing the next day to perform sampling and infusions out of reach from the rats. In this way, blood sampling was performed simultaneous with AMP-DNM or vehicle ig infusions, without stressing the animals. After 10 minutes of the AMP-DNM (100 mg/kg) or vehicle ig infusions, food was given back and 2h later food intake was measured. Blood samples for plasma GLP1 concentration assessment were taken at -60, 20, 40, and 60 minutes after infusions.

Oral glucose tolerance test. After 4 hours fasting, a basal blood sample was taken by a tail cut, followed by a 20% D-glucose oral gavage bolus (1 g/kg, D-glucose was obtained from Sigma, St Louis, USA). Blood samples were taken at 5, 10, 15, 30, 60 and 120 minutes after the glucose bolus and glucose was assessed by a glucometer (Freestyle, Abbott, Hoofdorp, The Netherlands). Area under the curve (AUC) was calculated using GraphPad Prism 6.

*GLP1 measurement.* Processed active forms of GLP1 were measured in blood samples and cell media immediately incubated in DPP-IV inhibitor Ile-Pro-Ile (Sigma, St Louis, USA) and kept on ice until centrifugation. After centrifugation, the plasma or cell media was stored at -80°C until measurement of active GLP1 by an ELISA (Millipore, Darmstadt, Germany).

BAT and brain immunohistochemistry. After perfusion of the mice with cold Phosphate-buffered saline (PBS), brains were removed and post fixed for 24 hours at 4°C in 4% paraformaldehyde diluted in PBS (0.1 M, pH 7.2). After this period the brains were cryoprotected in 30% sucrose for 2 days. Sections (35 μm) were cut and immunohistochemistry for C-Fos (1:750, Santa Cruz Biotechnology, Santa Cruz, CA) was performed as previously described (1). Immunofluorescence was also performed for C-Fos, POMC (Millipore, MA, USA) and GLP1 (Abcam, Cambridge, UK). Free floating sections were incubated overnight with primary antibodies for goat c-Fos (1:750), rabbit POMC (1:1000) and rabbit GLP1 (1:500). The next day, the brain sections were rinsed 3 times in TBS containing 0.5% (v/v) for 10 min. Secondary antibodies (1:1000) conjugated with fluorescent dyes: donkey anti-goat Alexa 594, donkey anti-sheep Alexa 488 and donkey anti-rabbit Alexa 488 were incubated for 2 hours. After rinsing, the sections were mounted and covered with DAPI and examined with a confocal laser scanning microscope (Leica SP5, Wetzlar, Germany).

Formalin-fixed paraffin-embedded BAT tissue sections (5µm) were stained with haematoxylin and eosin (H&E). Other sections were stained for Tyrosine hydroxylase (TH, 1:2000; Abcam, Cambridge, UK) as previously described (2).

Quantification of H&E signal, C-Fos and TH IR. 20X images of 6-8 coronal sections of the ARC, DMH and NTS were taken using an Axioskop microscope with scanning table (Zeiss, Jena, Germany) equipped with a black and white CCD camera (Sony XC-77, Tokyo, Japan), using the program Image-Pro Plus 6.3 (Media Cybernetics, MD, USA). After manually outlining the area covered by the ARC, DMH and NTS, the C-fos mask area was calculated using software developed at the Netherlands Institute for Neuroscience as previously described (3). The area covered by C-Fos mask was corrected by the total area covered by the ARC, DMH and NTS, finally percentages were calculated. The areas occupied by intracellular lipid vacuoles (H&E staining) and TH protein content were quantified using ImageJ.

Laser capture microdissection procedures. C57Bl/6J and ob/ob mice frozen brains were cut in 20 μm coronal sections, attached to PEN slides 1.0 mm (Zeiss, Gottingen, Germany) and stored at -80°C until

the moment of laser dissection. All working surfaces were treated with RNaseZAP (Sigma, St Louis, USA) and all glassware was baked at 280°C overnight to inactivate RNases. Just before the laser capture microdissection (LCM), the sections were stained with 0.1% cresyl violet for 45 seconds and rinsed briefly in RNase free H<sub>2</sub>O. Afterwards the tissue was dehydrated in 70% and 90% EtOH for 30 seconds each, followed by 1-minute dehydration in 100% EtOH. After 1 minute EtOH evaporation, ARC, DMH, LH and NTS were dissected using a PALM microdissection microscope (ZEISS, Gottingen, Germany). The dissected nuclei were stored in Trizol Reagent (Life Technologies, California, USA) in RNase free adhesive caps (ZEISS, Gottingen, Germany) at -80°C until further RNA isolation. In addition, whole hypothalamus (HT) and brainstem (BT) were dissected from GLP1r KD<sup>ΔNkx2.1</sup> and *wt* mice for RNA isolation.

Dissection of brain areas. GLP1r<sup>Nkx2.1</sup> KO and wt mice brainstems were isolated from the rest of the brain by separating the hindbrain from the cortical lobes at the level of inferior colliculus. The pons and cerebellum were separated from the brainstem and the brainstems were cut slightly lower of the obex to separate it from the spinal cord. The hypothalamus was dissected by introducing blunt curved forceps at the level of the mammillary nucleus and separating it from the rest of the brain.

RNA isolation and RT-PCR. RNA from the LCM brain nuclei was isolated after tissue homogenization with Trizol by vortexing repeatedly for a few seconds. RNase free chloroform was added and the transparent RNA phase was taken in a new RNAse free tube where isopropanol was added and stored at 4°C overnight for RNA precipitation. After centrifugation, the pellet was washed with 75% EtOH and air-dried until solubilization. RNA isolation of mice brown adipose tissue, hypothalamus and brainstem was performed as previously described (4). cDNA was synthesized according to the instruction of Invitrogen cDNA synthesis kit and gene expression analysis was performed using a Bio Rad MyIQ Real Time PCR detection system. The expression levels were normalized to the mean of P0 and GAPDH expression levels. The primers used for each gene investigated are presented in Table S1.

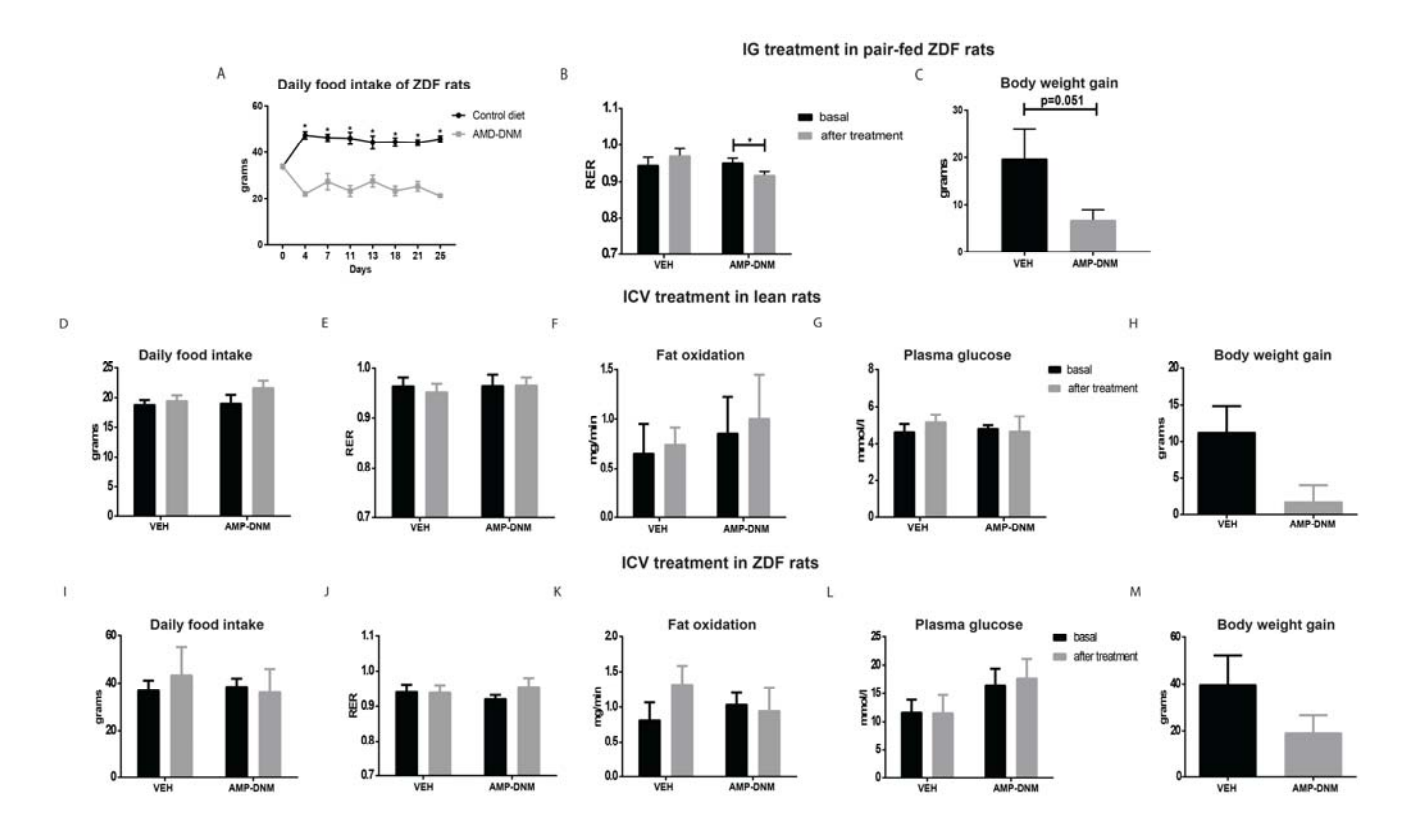
Generation of STC1 bitter taste receptor overexpressing cells. Human taste receptor type 2, member 16 (hT2r16, NM 016945.2) coding sequence was amplified using primers presented in Table S2 and subsequently cloned into the donor vector pDNOR221 using the Gateway system (Invitrogen, California, USA) and finally subcloned into the expression vector pcDNA3.1/Myc-His (Invitrogen, California, USA). In parallel, the first 45 amino acids of rat Somatostatin type 3 receptor (SSTR3) were cloned into the expression vector pcDNA3.1/Myc-His (Invitrogen, California, USA) and after digestion, fused with the hT2R16 (SSTR3-hT2R16) for cell surface targeting as previously described (5). For overexpression of the mouse taste receptor type 2, member 118 (T2R118, NM 207022.1), T2R118 coding sequence was amplified using primers presented in Table S2, in which a Nhe restriction site was added. The T2R118 digested fragment was subsequently ligated to previously SSTR3-hT2R16 digested fragment at the Nhe restriction site, to fuse SSTR3-T2R118 pcDNA3.1/Myc-His expression. STC1 cells were transfected with a construct for expression of either the "wild type" (wt) SSTR3 fusion protein and a construct with a Myc-tag for verification of overexpression of the taste receptor proteins. Overexpression confirmation was assessed after selection with Geneticin (Thermo Fisher Scientific, MA. USA) for several weeks. Rendered cells stably expressing the wt SSTR3-hT2R16 and wt SSTR3-T2R118 and the SSTR3-hT2R16-Myc and SSTR3-T2R118-Myc were lysed to examine mRNA expression by RT-PCR and protein expression by Western blot (data not shown).

Cell culture and functional intracellular Ca<sup>2+</sup> assays. hT2R16 and GFP STC1 stable cell lines were cultured in DMEM high glucose (Life Technologies, MA, USA) with 10% fetal bovine serum and maintained at 37°C under 5% CO<sub>2</sub>. The stable cell lines were divided to 60% confluency and the following day washed in Hanks' balanced salt solution (HBSS, Sigma, St Louis, USA) containing 10

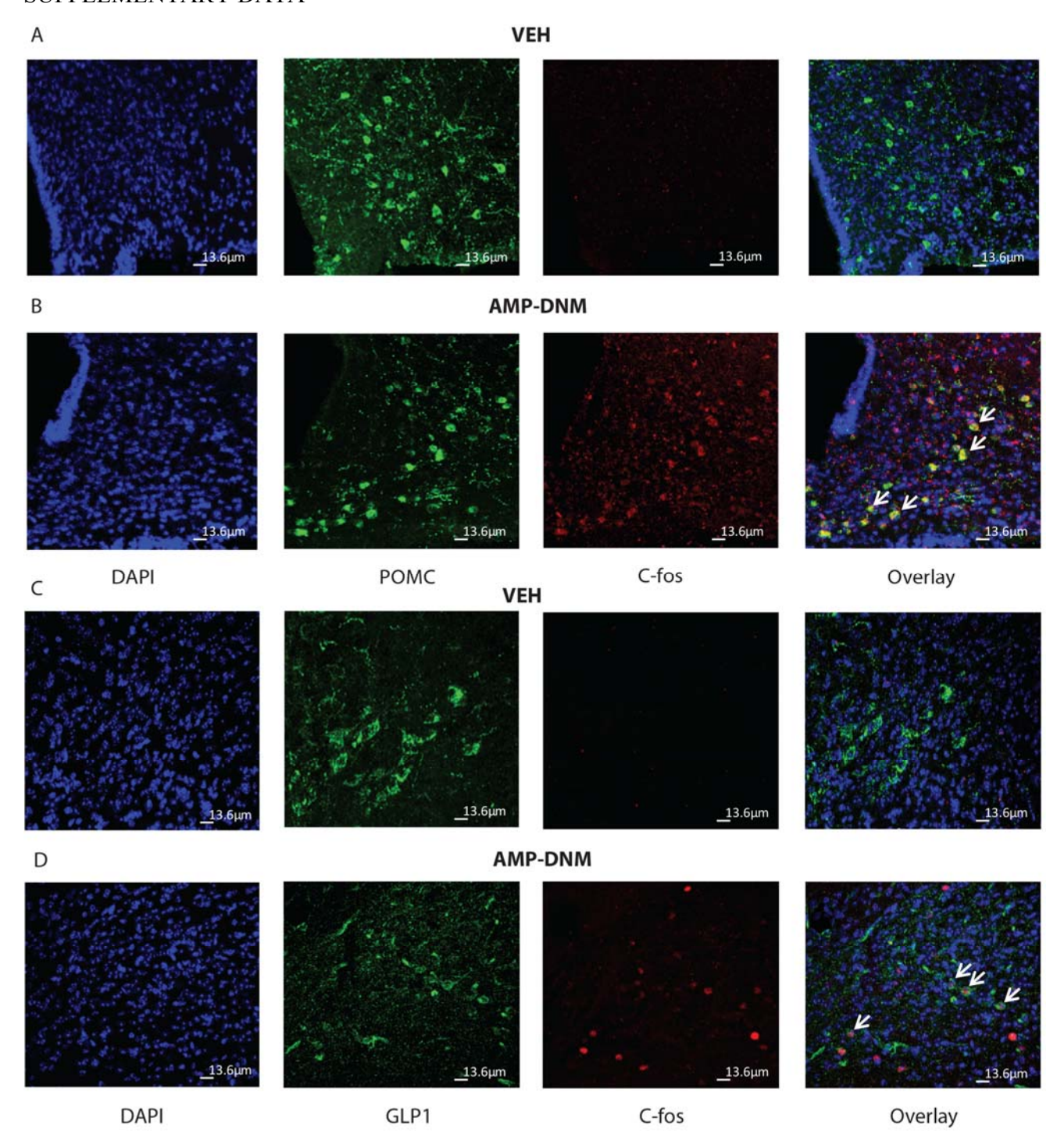
mM HEPES (Sigma, St Louis, USA) and then incubated with 10 μM Fluo-4-AM (Molecular Probes, Thermo Fisher Scientific, MA, USA) for 30 minutes at room temperature in the dark. The cells were washed again with HBSS and incubated for additional 30 minutes at 37°C for de-esterification of Acetoxymethyl esters. Fluorescent intracellular calcium assays were performed in a Synergy HTX Multi-Mode reader (Biotek, Vermont, USA), using excitation at 488 nm and emission at 515 nm. Final concentrations of L-glutamate (33 mM and 80 mM; Sigma, St Louis, USA), D-Salicin (1 mM and 10 mM; Sigma, St Louis, USA), AMP-DNM (0, 10, 50, 70 and 100 μM) and L-ido-AMP-DNM (0, 10, 50, 70 and 100 μM) were then applied to the cells. Basal fluorescent background was recorded for 1 minute and after compound application, fluorescent was measured for an additional 8 minutes. Fluorescent responses were measured every second after ligand administration and then corrected for the initial background fluorescence. Fluorescent differences were expressed as delta arbitrary fluorescent units (AFU), which was defined as the difference between the maximum and minimum fluorescent values in every assay (6). Finally, the medium was collected for further active GLP1 assessment.

Statistical analysis. Variance equality was tested by Levene's test. Significant values were set at p<0.05. Active GLP1 and OGTT glucose concentrations were analyzed by an ANOVA of repeated measures with 2 between subject factors: *Genotype* and *Substance*. An adjustment of Bonferroni was performed with significant values set as p<0.05.

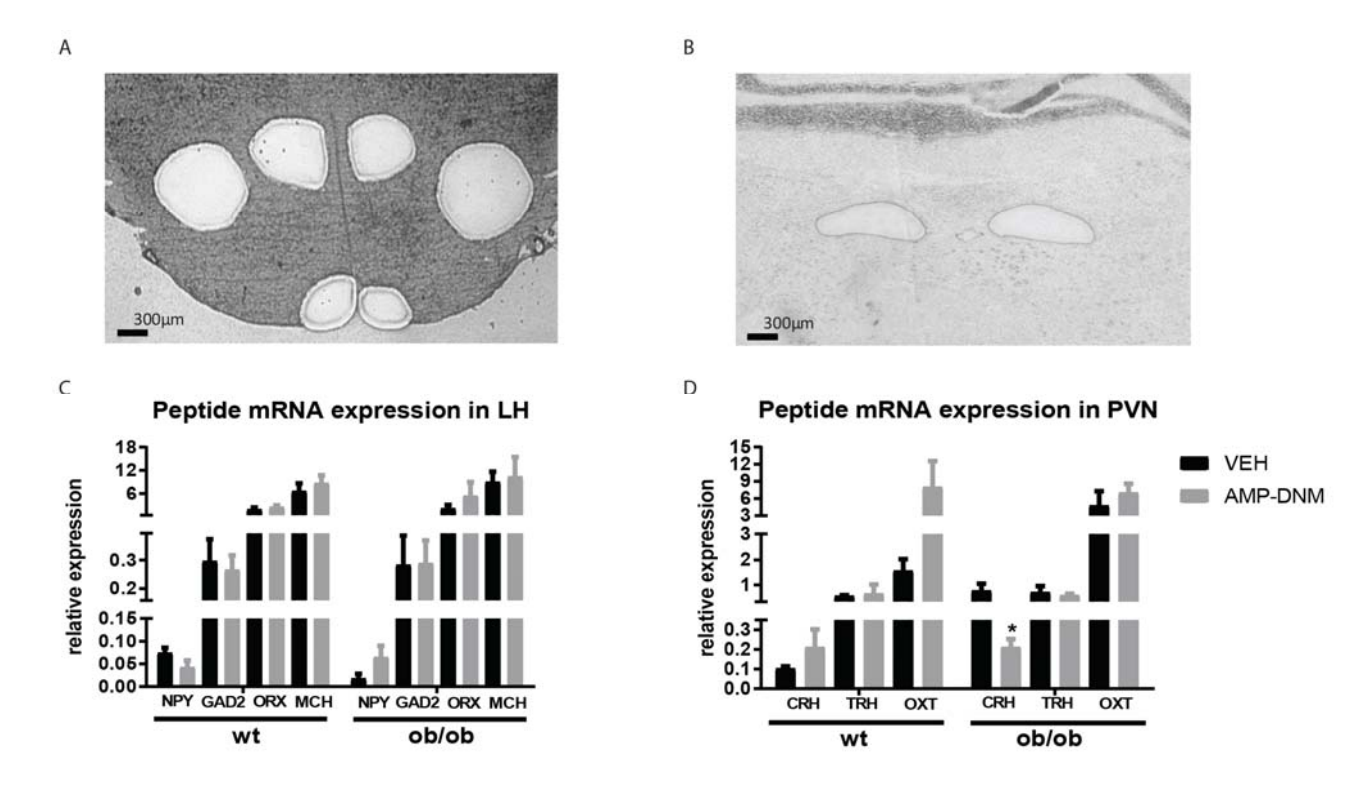
Supplementary Figure 1. Brain AMP-DNM administration does not modify metabolism in lean and obese ZDF rats. A) Daily food intake of obese ZDF rats after chronic ingestion of control diet or diet containing AMP-DNM. B) RER after AMP-DNM ig administration in obese pair-fed ZDF rats. C) Body weight gain after AMP-DNM ig administration in obese pair-fed ZDF rats. D) Daily food intake after AMP-DNM icv administration in lean rats. E) RER after AMP-DNM icv administration in lean rats. F) Fat oxidation rate after AMP-DNM icv administration in lean rats. G) Plasma glucose levels after AMP-DNM icv administration in lean rats. H) Body weight gain after AMP-DNM icv administration in obese ZDF rats. J) RER after AMP-DNM icv administration in obese ZDF rats. K) Fat oxidation rate after AMP-DNM icv administration in obese ZDF rats. K) Plasma glucose levels after AMP-DNM icv administration in obese ZDF rats. VEH refers to vehicle administration.



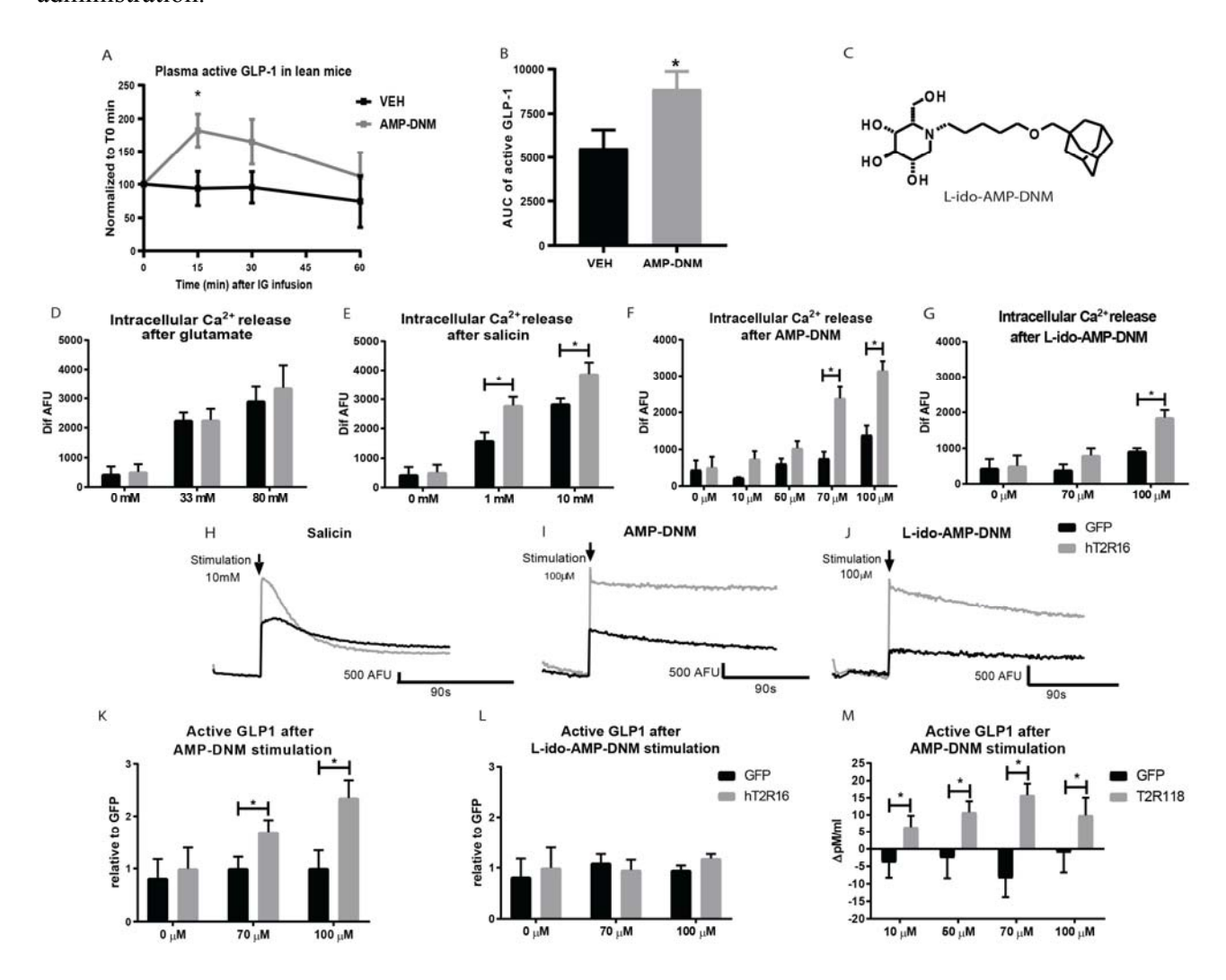
**Supplementary Figure 2.** AMP-DNM activates POMC neurons in the ARC and GLP1 neurons in the NTS. A) Double immunofluorescence of C-Fos (red) and POMC (green) immunoreactivity in the ARC of ob/ob mice ig infused with vehicle. Cell nuclei are shown in DAPI (blue). B) Double immunofluorescence of C-Fos (red) and POMC (green) immunoreactivity in the ARC of ob/ob mice ig infused with AMP-DNM. Cell nuclei are shown in DAPI (blue). Some POMC neurons show C-Fos after AMP-DNM administration. C) Double immunofluorescence of C-Fos (red) and GLP1 (green) immunoreactivity in the NTS of ob/ob mice ig infused with vehicle. Cell nuclei are shown in DAPI (blue). D) Double immunofluorescence of C-Fos (red) and GLP1 (green) immunoreactivity in the NTS of ob/ob mice ig infused with AMP-DNM. Cell nuclei are shown in DAPI (blue). Some GLP1 neurons show C-Fos after AMP-DNM administration. VEH refers to vehicle administration.



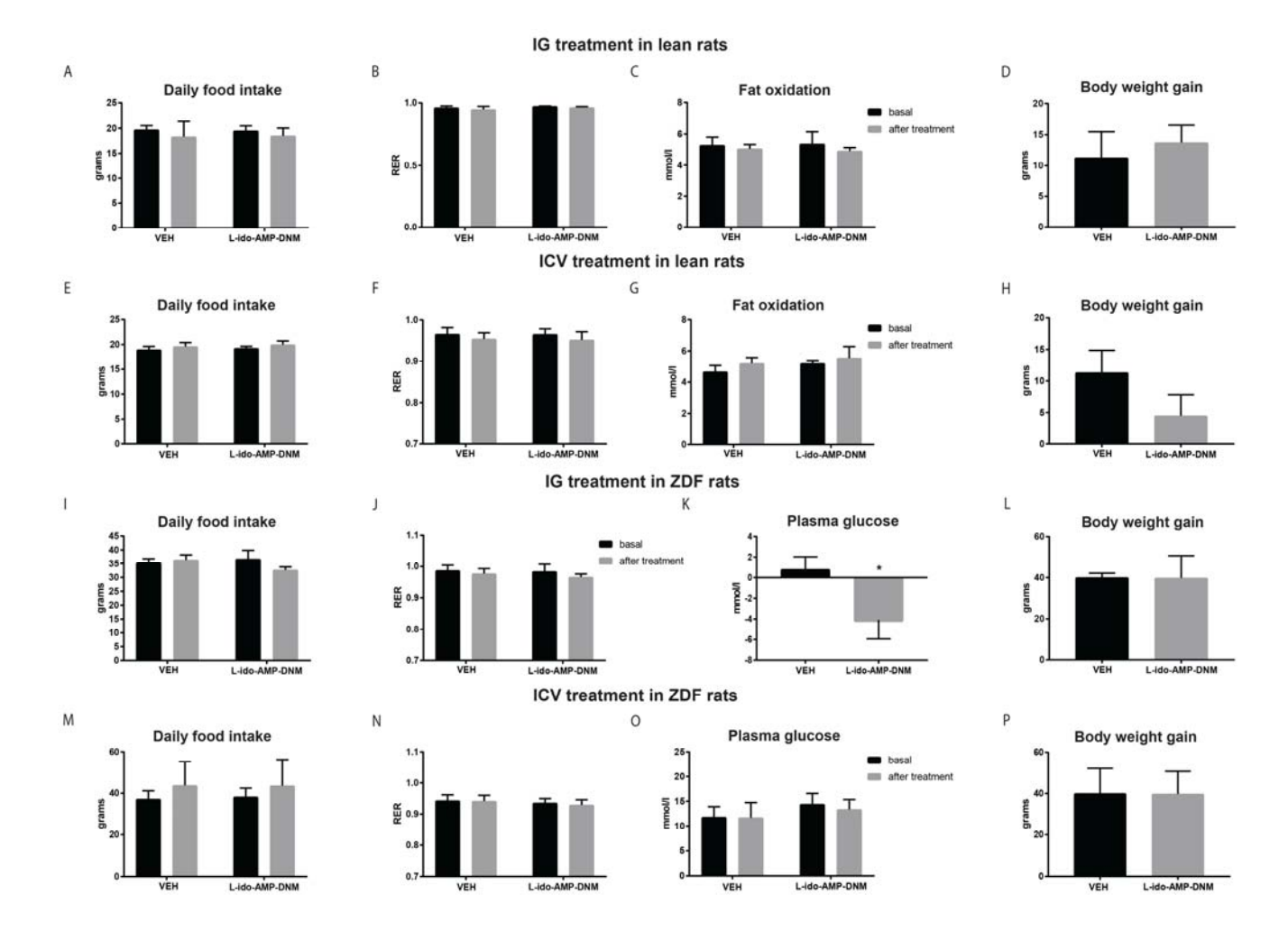
**Supplementary Figure 3. A)** Representative image of laser capture microdissection (LCM) of ARC, DMH and LH. **B)** Representative image of LCM of NTS. **C)** Neuropeptide mRNA expression in the LH. **D)** Neuropeptide mRNA expression in the PVN. VEH refers to vehicle administration.



**Supplementary Figure 4. AMP-DNM stimulates intestinal GLP1 secretion by entero-endocrine STC1 cells through bitter receptor hT2R16 and T2R118. A)** Plasma GLP1 after AMP-DNM ig in lean mice. **B)** Area under the curve (AUC) of plasma GLP1 during 60 min after AMP-DNM ig in lean mice. **C)** Chemical structure of L-ido-AMP-DNM. **D)** Dif AFU after glutamate stimulation 6 of GFP and hT2R16 overexpressing cells. **E)** Dif AFU after salicin stimulation of GFP and hT2R16 overexpressing cells. **G)** Dif AFU after L-ido-AMP-DNM stimulation of GFP and hT2R16 overexpressing cells. **H)** Representative Ca<sup>2+</sup> traces induced by salicin in GFP and hT2R16 overexpressing cells. **J)** Representative Ca<sup>2+</sup> traces induced by AMP-DNM in GFP and hT2R16 overexpressing cells. **J)** Representative Ca<sup>2+</sup> traces induced by L-ido-AMP-DNM in GFP and hT2R16 overexpressing cells. **K)** Medium GLP1 after AMP-DNM stimulation of GFP and hT2R16 overexpressing cells. **L)** Medium GLP1 after L-ido-AMP-DNM stimulation of GFP and hT2R16 overexpressing cells. **M)** Medium GLP1 after L-ido-AMP-DNM stimulation of GFP and hT2R16 overexpressing cells. **VEH** refers to vehicle administration.



Supplementary Figure 5. L-ido-AMP-DNM does not modify metabolism in lean and obese ZDF rats. A) L-ido-AMP-DNM or vehicle was administered by gavage (ig). Daily food intake of lean rats. B) RER of lean rats. C) Plasma glucose levels of lean rats. D) Body weight gain of lean rats. E) L-ido-AMP-DNM or vehicle was administered intracerebroventricularly (icv). Daily food intake of lean rats. F) RER of lean rats. G) Plasma glucose levels of lean rats. H) Body weight gain of lean rats. I) L-ido-AMP-DNM or vehicle was administered by gavage (ig). Daily food intake of obese ZDF rats. J) RER of ZDF rats. K) Plasma glucose levels of ZDF rats. L) Body weight gain in ZDF rats. M) L-ido-AMP-DNM or vehicle was administered intracerebroventricularly (icv). Daily food intake of lean rats. N) RER of ZDF rats. O) Plasma glucose levels of ZDF rats. P) Body weight gain in ZDF rats. VEH refers to vehicle administration.



**Supplementary Table 1.** Primers used for RT-PCR of BAT activation marker mRNA expression in mice BAT and neuropeptide mRNA expression in LCM and dissected mice brain areas.

	<b>BAT</b> activation markers	
Uncoupling protein 1 ( <i>Ucp-1</i> )	Fwd: 5'-tgtgctttgaacagctgaaaa-3'	Rev: 5'-tggtctcccagcatagaagc-3'
Peroxisome proliferated activated receptor, gamma, coactivator 1 alpha ( <i>Pgc-1α</i> )	Fwd: 5'- caaagcagcagagagggaac-3'	Rev: 5'-gccatcaaaaagggacacat-3'
Нуро	thalamic and brainstem neurope	eptides
Neuropeptide Y (NPY)	Fwd: 5'-agagatecagecetgagaca-3'	Rev: 5'-gatgagggtggaaacttgga-3'
Agouti related protein (AgRP)	Fwd: 5'- gcagaccgagcagaagaagt-3'	Rev: 5'-gactcgtgcagccttacaca-3'
Pro-opimelanocortin (POMC)	Fwd: 5'- agttcaagagggagctggaag-3'	Rev: 5'-ggtcatgaagccaccgtaac-3'
Glutamic acid decarboxylase 2 ( <i>GAD2</i> )	Fwd: 5'-cattggggtaatggaaatcg-3'	Rev: 5'-cgatttccattaccccaatg-3'
Orexin (ORX)	Fwd: 5'-tagagecacatecetgetet-3'	Rev: 5'-gggaagtttggatcaggaca-3'
Pro-melanin-concentrating hormone ( <i>MCH</i> )	Fwd: 5'-cccagctgagaatggagtt-3'	Rev: 5'-gccaacatggtcggtagact-3'
Preproglucagon (PPG)	Fwd: 5'-tgacgagatgagcaccattc - 3'	Rev: 5'-ggcacgagatgttgtgaaga - 3'

Supplementary Table 2. Primers used for taste receptor member coding sequence amplification.

Human taste receptor type 2, member 16 (hT2R16)		
Sense primer	5'-ggggacaagtttgtacaaaaaagcaggctgccgccaccatggccgct-3'	
Antisense primer for <i>wt</i> coding sequence	5'-ggggaccactttgtacaagaaagctgggttcaatggtgatggtgatgatg-3'	
Antisense primer for coding sequence with a stop codon	5'-ggggacccactttgtacaagaaagctgggttcactagcactttccctttagaatcc-3'	
Mouse taste	receptor type 2, member 118 (T2R118)	
Sense primer	5'-catgctagctgtcagtggcatggtgccaacgcaagtcac-3'	
Antisense primer for <i>wt</i> coding sequence	5'-catcatgcggccgcggaaggctctgggctcca-3'	
Antisense primer for coding sequence with a stop codon	5'-catcatgcggccgctcaggaaggctctgggctc-3'	

#### References

- 1. Chao DH, Leon-Mercado L, Foppen E, Guzman-Ruiz M, Basualdo MC, Escobar C, Buijs RM: The Suprachiasmatic nucleus modulates the sensitivity of Arcuate nucleus to hypoglycemia in the male rat. Endocrinology 2016:en20151751
- 2. Kooijman S, Wang Y, Parlevliet ET, Boon MR, Edelschaap D, Snaterse G, Pijl H, Romijn JA, Rensen PC: Central GLP-1 receptor signalling accelerates plasma clearance of triacylglycerol and glucose by activating brown adipose tissue in mice. Diabetologia 2015;58:2637-2646
- 3. Goncharuk VD, Buijs RM, Jhamandas JH, Swaab DF: The hypothalamic neuropeptide FF network is impaired in hypertensive patients. Brain Behav 2014;4:453-467
- 4. Herrera Moro Chao D, Argmann C, Van Eijk M, Boot RG, Ottenhoff R, Van Roomen C, Foppen E, Siljee JE, Unmehopa UA, Kalsbeek A, Aerts JM: Impact of obesity on taste receptor expression in extra-oral tissues: emphasis on hypothalamus and brainstem. Sci Rep 2016;6:29094
- 5. Greene TA, Alarcon S, Thomas A, Berdougo E, Doranz BJ, Breslin PA, Rucker JB: Probenecid inhibits the human bitter taste receptor TAS2R16 and suppresses bitter perception of salicin. PLoS One 2011;6:e20123
- 6. Sakurai T, Misaka T, Ueno Y, Ishiguro M, Matsuo S, Ishimaru Y, Asakura T, Abe K: The human bitter taste receptor, hTAS2R16, discriminates slight differences in the configuration of disaccharides. Biochem Biophys Res Commun 2010;402:595-601